

Scaling limit of domino tilings on a pentagonal domain

Filippo Colomo and Andrei G. Pronko

ABSTRACT. We consider the six-vertex model at its free-fermion point with domain wall boundary conditions, which is equivalent to random domino tilings of the Aztec diamond. We compute the scaling limit of a particular non-local correlation function, essentially equivalent to the partition function for the domino tilings of a pentagon-shaped domain, obtained by cutting away a triangular region from a corner of the initial Aztec diamond. We observe a third-order phase transition when the geometric parameters of the obtained pentagonal domain are tuned to have the fifth side exactly tangent to the arctic ellipse of the corresponding initial model.

1. Introduction

Random tilings of regular lattices and related dimer models possess numerous fascinating features, among those, perhaps, most intriguing and important are phase separation phenomena. A seminal example is provided by the tilings of an hexagon by lozenges (rhombi), which are in bijection with boxed plane partitions [1]. Another classic instance is given by the random tilings of the ‘Aztec diamond’ by dominoes, where one can observe ordered, or ‘frozen’, configurations in the four corners, outside a central disordered region. The phase separating curve resulting in the scaling limit is named arctic circle, or, for a weighted counting of configurations, arctic ellipse [2, 3]. In rather general settings these problems can be studied in the framework of dimer models [4, 5].

Phase separation phenomena may be also observed in vertex models, which can be viewed as interacting generalizations of dimer models [6, 7]. In particular, when the parameters (Boltzmann weights) of the vertex models are tuned to the non-interacting case, these can be used as an alternative tool to study random tilings. Consequently, many results obtained in the context of the vertex models find application in various problems in combinatorics and related areas, including the theory of symmetric polynomials, see, e.g., [8, 9] and references therein.

As an example, one can consider the domino tilings of the Aztec diamond with a cut-off corner of macroscopic square shape and given size, and study the bulk properties of the tilings as the size is varied [10]. In this problem one can rely on the well-known correspondence between the domino tilings of the Aztec diamond and the six-vertex model with domain wall boundary conditions (DWBC) [6, 7, 11]. In [10], this correspondence have been applied to study thermodynamics of the domino tilings of the Aztec diamond with a cut-off corner of a square shape. The six-vertex model have been considered with a square portion of the lattice removed, again

with DWBC, and the resulting domain has the L-letter shape [12]. The Boltzmann weights have to be chosen to obey the free-fermion condition.

In the present paper, we apply similar ideas to study thermodynamics of the domino tilings of the Aztec diamond with a cut-off corner of a triangular shape, the resulting domain having a pentagonal shape. Our main result is the expression for the free energy of the random domino tilings of the resulting region. It is worth mentioning that domino tilings of a pentagonal domain has already been considered in [13], see also [14]. However the focus there was rather on a discrete microscopic derivation of the hard-edge tacnode process [15].

We use the observation [16] that the partition function of the six-vertex model on a modified lattice can be written as certain non-local correlation function of the six-vertex model on the original lattice with DWBC. To obtain a cut-off corner of rectangular shape one has to consider the correlation function known as the emptiness formation probability (EFP), which can be viewed as a test function for total ferroelectric order in a rectangular sub-region in a corner of the original lattice. To extend these ideas to a cut-off corner of arbitrary shape, one can introduce the generalized emptiness formation probability (GEFP) [17]. Under certain choice of the geometric parameters, it can produce a cut-off region of generic shape, for example, a triangular one. Here, we focus on this case and derive the behavior of GEFP in the thermodynamic limit, for the free-fermion Boltzmann weights.

We use the method of log-gas to derive the free energy, or, equivalently, the leading term of the logarithm of the GEFP, following the techniques exposed in detail in [10, 12]. It has to be noted that in the case of EFP, related to domino tilings of the L-shaped domain, there exists a connection to the theory of the sixth Painlevé equation, which makes it possible to build thermodynamic limit asymptotic expansions up to an arbitrary order in the large parameter [18]; see also [19], where an application of this method to the five-vertex model with scalar-product boundary conditions was considered. For the pentagonal domain such a connection is unknown. Nevertheless, a random-matrix-like formula is available for the partition function [20], which, despite some relevant difference, may actually be treated with random matrix model technologies. We use this formula as the starting point in our considerations here.

Restating the result in terms of tilings, we get the free energy density for the domino tilings of the Aztec diamond with a triangular cut-off corner, as a function of the size of the cut-off triangle. We observe that the free energy displays a third-order phase transition of Douglas–Kazakov type [21], when the geometric parameters of the obtained pentagonal domain are tuned to have the fifth side exactly tangent to the arctic ellipse, that is the phase separation curve of the original (unmodified) Aztec diamond. In other words, phase separation curves can be viewed as critical curves in the space of parameters describing the macroscopic geometry of the tiled region [10, 12].

2. The generalized emptiness formation probability

We consider the six-vertex model on the $N \times N$ lattice. This means that the lattice is obtained from the intersection of N horizontal and N vertical lines. The configurations of the model are obtained by orienting the edges (placing arrows on them), with the condition that around each vertex two arrows point inward and two outward. This condition is known as the ice rule, and allows for exactly six possible

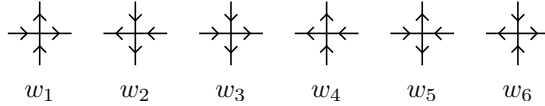


FIG. 1. Arrow configurations around a vertex (first row) and the corresponding vertex Boltzmann weights (second row).

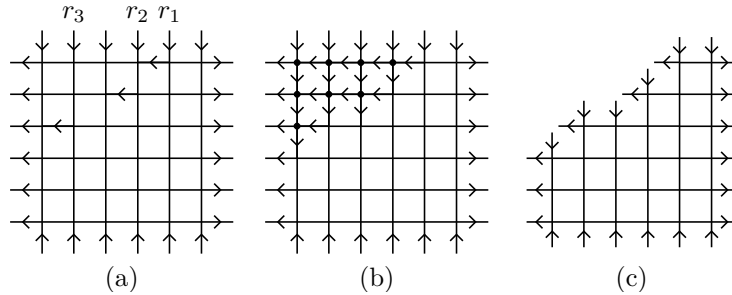


FIG. 2. GEFP for the $N \times N$ lattice: (a) The configuration of arrows, whose probability is described by GEFP; (b) The Ferrer diagram λ_s associated with the “frozen” region with dots standing for vertices of type 2; (c) The cut-off domain obtained by removing the vertices forming λ_s . Here $N = 6$, $s = 3$, $(r_1, r_2, r_3) = (2, 3, 5)$, and $\lambda_s = (4, 3, 1)$.

vertex configurations, to which we assign the Boltzmann weights w_j , $j = 1, \dots, 6$, as in Fig. 1.

We consider the model with DWBC, that is, we require the arrows to point outward on the horizontal external edges, and inward on the vertical ones [11, 22, 23]. We label the vertex at the intersection of the r th vertical line (counted from the right) and the s horizontal line (counted from the top) by the lattice coordinates (r, s) , with $r, s = 1, \dots, N$. The partition function is defined as the sum over all possible configurations of arrows on the lattice, satisfying the ice-rule and the boundary conditions.

To define the GEFP, let us consider the set of s horizontal edges $\{e_1, \dots, e_s\}$, where $s \leq N$, with the edge e_j lying to left of the vertex of coordinates (r_j, j) , $j = 1, \dots, s$. The r_j ’s are required to be a weakly increasing sequence, $1 \leq r_1 \leq \dots \leq r_s \leq N$. Note that one may associate to the above set of edges an s -row Ferrer diagram, defined by the partition $\lambda_s = (N - r_1, \dots, N - r_s)$.

The GEFP, denoted $G_{N,s}^{(r_1, \dots, r_s)}$, is defined as the probability of having the arrows on the s horizontal edges e_1, \dots, e_s all pointing leftward, see Fig. 2a. The GEFP may equivalently be defined as the probability of observing in the top-left corner of the $N \times N$ lattice a frozen region of shape λ_s , with all vertices therein being of type 2, see Fig. 1b. The equivalence of the two definitions follows from both the ice-rule and the DWBC. Note that, the top-left corner being frozen, it may as well be cut away, allowing to relate GEFP directly to the partition function of the six-vertex model on a quite general class of domain on the square lattice, still with domain wall boundary conditions, see Fig. 2c.

It follows from the definition of GEFP that it may be evaluated as the ratio between two different partition functions of the model: one with the boundary conditions implementing the freezing of the assigned Ferrer diagram, and one with DWBC. In [17], a multiple integral representation has been derived for GEFP, by computing these two partition functions in the framework of the quantum inverse scattering method [24].

When the r_j 's are chosen to be all equal to r , the GEFP reduces to the EFP, $F_N^{(r,s)} \equiv G_{N,s}^{(r,\dots,r)}$, giving the probability of observing a frozen rectangle of size $(N-r) \times s$ in the top-left corner of the lattice. Clearly in this case some simplifications occur, allowing for the derivation of various multiple integral representations [16, 25–27], and for an analytic treatment of their behaviour in the scaling limit [28]. If one further specialize $r = N - s$, the frozen region becomes an $s \times s$ square, with additional simplifications allowing for the derivation of some more explicit results [29].

Another interesting situation, allowing for some simplification as well, is that in which the region required to be frozen, and the corresponding Ferrer diagram, have a triangular shape. This is realized by specializing $r_j = N - s + j - 1$, $j = 1, \dots, s$, with $s < N$. We may thus define the Triangular Domain EFP (TDEFP),

$$T_{r,s} := G_{N,s}^{(N-s, N-s+1, \dots, N-1)}, \quad r+s = N,$$

giving the probability of observing in the top-left corner of the $N \times N$ lattice, a frozen triangular region of size s [20].

The problem we want to address is to investigate TDEFP in the scaling limit, for the six-vertex model at its free-fermion point. As a by-product, we derive the free energy per site of the six-vertex model on a pentagonal domain, or, equivalently, the free energy for domino tilings of the pentagonal domain, that we will exposed in detail below.

3. The free-fermion case

In what follows we restrict ourselves to the case where the Boltzmann weights obey the free-fermion condition:

$$w_1 w_2 + w_3 w_4 = w_5 w_6. \quad (3.1)$$

Under this condition, the partition function of the six-vertex model on the $N \times N$ lattice with DWBC, Z_N , takes a very simple form, see, e.g., [6, 7]:

$$Z_N = w_5^{\frac{N(N-1)}{2}} w_6^{\frac{N(N+1)}{2}}. \quad (3.2)$$

We parameterize the Boltzman weights as follows:

$$w_1 = w_2 = \sqrt{\rho(1-\alpha)}, \quad w_3 = w_4 = \sqrt{\rho\alpha}, \quad w_5 = 1, \quad w_6 = \rho. \quad (3.3)$$

Recall that, due to the DWBC, in any given configuration of the model the number of vertices of type 6 minus that of type 5 equals N . Consequently, the parameter ρ is just an overall normalization of weights. Instead, the parameter $\alpha \in [0, 1]$ is relevant, favoring the occurrence of vertices of type 1 and 2 ($\alpha < 1/2$), or of type 3 and 4 ($\alpha > 1/2$).

Under the free-fermion condition (3.3), the multiple integral representation for the GEFP simplifies significantly, and may be rewritten as a determinant, see [20],

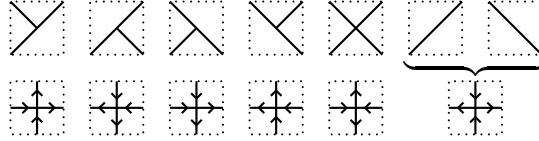


FIG. 3. Patches of domino tilings (first row) and corresponding vertices of the six-vertex model (second row).

Eq. (6). One has:

$$G_{N,s}^{(r_1, \dots, r_s)} = \left(\prod_{j=1}^s (1-\alpha)^{N-r_j} \right) \det_{1 \leq j, k \leq s} \left[P_{N-s+j+k-2}^{(N-r_{s-j+1}, j)}(\alpha) \right] \quad (3.4)$$

with

$$P_l^{(m,n)}(\alpha) := \oint \frac{x^l}{(x-\alpha)^m (x-1)^n} \frac{dx}{2\pi i},$$

where the integration is taken over a positive contour enclosing the poles at α and 1. It may be verified that $P_l^{(m,n)}(\alpha)$ is a polynomial of degree $l - m - n + 1$ in α .

In the case of TDEF, (3.4) simplifies further, and various alternative representations have been proposed in [20]. Below we shall resort to two of them. The first one follows directly from the determinantal representation (3.4) by specializing $r_j = N - s + j - 1$,

$$T_{r,s} = (1-\alpha)^{s(s+1)/2} \det_{1 \leq j, k \leq s} \left[P_{r+j+k-2}^{(j,j)}(\alpha) \right], \quad (3.5)$$

and we recall that $r \equiv r_1 = N - s$.

The second representation reads:

$$T_{r,s} = (1-\alpha)^{s(s+1)/2} \sum_{0 \leq m_1 \leq \dots \leq m_s < r} \prod_{j=1}^s \alpha^{m_j} \prod_{1 \leq j < k \leq s} \frac{2m_k - 2m_j + k - j}{k - j}. \quad (3.6)$$

This expression may remind the partition function of some discrete log-gas, despite some relevant difference. Actually it exhibits strong similarities with the partition function for pure continuous Yang-Mills theory on the two-sphere [21], and may similarly be treated by resorting to random matrix model technologies.

4. The six-vertex model and domino tilings

Let us here recall the correspondence between the six-vertex model on a square lattice and the domino tilings [6, 7]. Given a generic tiling, it may be decomposed into elementary patches, that may be mapped into arrow configurations of the six-vertex model as shown in Fig. 3. The Aztec diamond of order N then corresponds to the six-vertex model on an $N \times N$ lattice with DWBC, see Fig. 4.

From Fig. 3, it is clear that two different elementary patches of domino tilings correspond to the same one vertex of type 6. It follows that the enumeration of all possible tilings of the Aztec diamond by dominoes is equal to the partition function of the six-vertex model with DWBC, with the following choice of Boltzmann weights: $w_1 = \dots = w_5 = 1$, and $w_6 = 2$. Indeed, with this choice of the weights one readily recovers from (3.2) the celebrated result $2^{N(N+1)/2}$, proven in [6, 7].

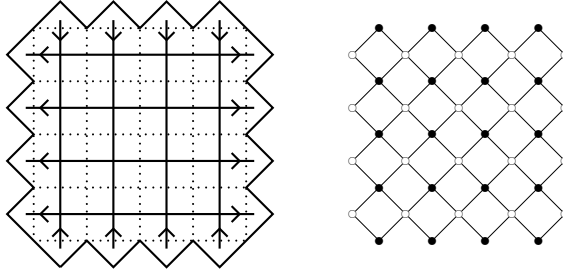


FIG. 4. An Aztec diamond of order 4 and the underlying 4×4 lattice with DWBC (left), and the related bipartite graph for dimer coverings (right).

Clearly, with the above choice, the Boltzmann weights satisfy the free-fermion condition (3.1), and correspond to the specialization $\rho = 2$ and $\alpha = 1/2$ in the parametrization (3.3). As mentioned above, ρ is simply an overall normalization of the Boltzmann weights, while $\alpha \in [0, 1]$ is relevant, parameterizing the different weights $\sqrt{2(1-\alpha)}$ or $\sqrt{2\alpha}$, given to dominoes according to their NE-SW, or NW-SE orientation, respectively [2].

Given an Aztec diamond of order $N = r + s$, we may remove from it s diagonal rows, $s < N$, starting from the top-left corner, see Fig. 5. We shall refer to the obtained region as the pentagonal domain, parameterized by the integers r and s , with $r = N - s$. Note that the cut-off triangular domain admits only one tiling, with all dominoes oriented in the NE-SW direction.

Consider now the six-vertex model on an $(r+s) \times (r+s)$ lattice with a frozen triangular portion of size s (consisting in $s(s+1)/2$ vertices of type 2) removed from the top-left corner. By construction, the resulting model still has DWBC, namely vertical external arrows are all incoming, and horizontal ones are all outgoing, including along the new boundary, see Fig. 5. We shall denote by $Z_{r,s}$ the partition function of the six-vertex model on such an obtained lattice. Clearly, $Z_{r,0} = Z_r$.

Due to the relation between vertex and domino configurations, Fig. 3, the six-vertex model on the restricted domain indeed translates into a pentagonal domain, modulo a comb-like structure constraining the configurations of dominoes adjacent to the slanted boundary, see Fig. 5.

We want to study the limit of large lattice sizes, with large sizes of the cut-off triangle, that is, we consider both r and s large, with their ratio fixed. For a later use, we introduce the parameter

$$\omega = \frac{s}{r+s}.$$

Since r and s are positive integers, $\omega \in (0, 1)$. The free energy per site of the model is defined as

$$F(\omega) := - \lim_{\substack{r,s \rightarrow \infty \\ s/(s+r) = \omega}} \frac{\log Z_{r,s}}{r^2 + 2rs + s(s-1)/2}. \quad (4.1)$$

The partition function of the six-vertex model on the pentagonal domain, $Z_{r,s}$, coincides, modulo a simple overall factor, with the TDEFP, see Fig. 2c. Indeed, even under generic choice of the Boltzmann weights, it follows from the definition of

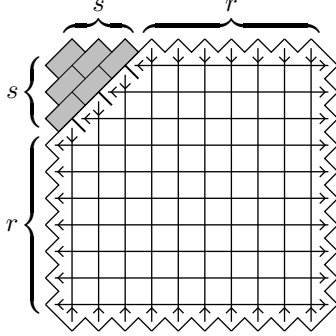


FIG. 5. The Aztec diamond of order $r+s$ of a pentagonal shape and the corresponding lattice of the six-vertex model with a cut-off triangle, for $r = 7$ and $s = 3$. Note the comb-like structure on the slanted side, constraining the position of dominoes along that boundary, and induced in the domino tiling picture by the vertices of type 2 in the triangular frozen region of the six-vertex model.

TDEFP that

$$Z_{r,s} = \frac{Z_{r+s}}{w_2^{s(s+1)/2}} T_{r,s}.$$

If we specialize the Boltzmann weights according to the parameterization (3.3), we get

$$Z_{r,s} = \frac{\rho^{(r+s)(r+s+1)/2 - s(s+1)/4}}{(1-\alpha)^{s(s+1)/4}} T_{r,s}. \quad (4.2)$$

In the scaling limit, that is, when r and s are both large, with the ratio $\omega = s/(r+s)$ fixed, the leading behaviour of TDEFP is described by the function

$$\sigma(\omega) := - \lim_{s \rightarrow \infty} \frac{1}{s^2} \log T_{\lceil (1/\omega - 1)s \rceil, s} \quad (4.3)$$

Some properties of the function $\sigma(\omega)$ follow from the definition of TDEFP. In particular, $T_{r,s}$ being a probability, it varies between 0 and 1, implying $\sigma(\omega) \geq 0$. Moreover, since the number of configurations contributing to the TDEFP may only decrease (or stay constant) as the ratio $s/(r+s)$ increases, $\sigma(\omega)$ is a non-decreasing function.

Recalling (3.2), (3.3), (4.2), and (4.3), we may thus write the free energy per site of the six-vertex model on the pentagonal domain (4.1) as follows

$$F(\omega) = -\log \sqrt{\rho} + \frac{\omega^2}{4 - 2\omega^2} \log(1 - \alpha) + \frac{2\omega^2}{2 - \omega^2} \sigma(\omega).$$

The free-energy density $F(\omega)$ is therefore completely determined by the function $\sigma(\omega)$, defined in (4.3), whose exact form will be derived below.

Let us conclude this Section by discussing the qualitative behaviour of the function $\sigma(\omega)$. Recall that the arctic circle (or ellipse) phenomenon in the domino tilings of the Aztec diamond is the appearance, in the scaling limit, of four regions of order, sharply separated from a central region of disorder. In the language of the six-vertex model, we thus have in the top-left corner, outside the arctic ellipse, a region with all its vertices of type 2. It follows, from its very definition, that TDEFP must be close to one as long as the triangular region of side s entirely lies

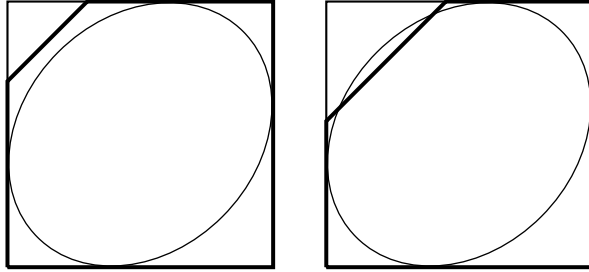


FIG. 6. Two scenarios for the thermodynamic limit, $r, s \rightarrow \infty$, shown schematically: the triangular region lies outside of (left) and overlaps with (right) the arctic ellipse of the original square domain. For the first case $\omega \in (0, \omega_c]$ and for the second case $\omega \in [\omega_c, 1)$, where $\omega = r/(r+s)$ and $\omega_c = 1 - \sqrt{\alpha}$. The border of the triangular region exactly touches the ellipse at the critical value $\omega = \omega_c$.

in the top-left frozen region [30]. In other words, as $r, s \rightarrow \infty$, the TDEFP tends to 1 when r and s are such that $s \ll r$, and tends to 0 when r and s , being of the same magnitude, are such that the triangular region overlaps with the central disordered region, see Fig. 6.

Concerning the function $\sigma(\omega)$, defined in (4.3), we thus expect it to vanish identically for $\omega \in (0, \omega_c]$, where the critical value $\omega_c = \omega_c(\alpha)$ corresponds to the diagonal side of the cut-off triangle being exactly tangent the arctic ellipse. From the known position of the arctic curve, corresponding for TDEFP to $s \sim (1 - \sqrt{\alpha})(r+s)$, we expect

$$\omega_c = 1 - \sqrt{\alpha}. \quad (4.4)$$

On the remaining interval, $\omega \in [\omega_c, 1)$, we expect the function $\sigma(\omega)$ to be positive-valued and non-decreasing. As we shall see, these features will be indeed observed in the explicit form of the function $\sigma(\omega)$, whose exact derivation we shall now address.

5. Scaling limit behaviour of TDEFP

5.1. Preliminaries. Our starting point is representation (3.6) for the TDEFP. We have

$$T_{r,s} = \left(\frac{1 - \alpha}{\sqrt{\alpha}} \right)^{s(s+1)/2} g_{r,s},$$

with

$$g_{r,s} := \alpha^{s(s+1)/4} \sum_{0 \leq m_1 \leq \dots \leq m_s < r} \prod_{j=1}^s \alpha^{m_j} \prod_{1 \leq j < k \leq s} \frac{2m_k - 2m_j + k - j}{k - j}.$$

where we have extracted a simple α -dependent factor for later convenience.

It is convenient to introduce the ‘shifted’ variable

$$h_j := 2m_j + j, \quad j = 1, \dots, s, \quad (5.1)$$

satisfying

$$\frac{h_k - h_j}{k - j} \geq 1.$$

in terms of which we may write

$$g_{r,s} \propto \sum_{0 < h_1 < \dots < h_s < 2r+s-1} \prod_{j=1}^s \alpha^{\frac{1}{2}h_j} \prod_{1 \leq j < k \leq s} (h_k - h_j). \quad (5.2)$$

Note that in the multiple sum, the h_j runs over even (odd) integers for even (odd) values of $j = 1, \dots, s$. In (5.2) we are ignoring an overall pre-factor, depending neither on r nor on α , but only on s , and whose explicit values is irrelevant for our purpose.

Now, since h_j is strictly increasing, the Vandermonde-like term is always positive (or vanishing, when $h_k = h_j$), and we may as well take its absolute value, obtaining a summand which is symmetric under interchange of its variables. However, the symmetrization of the sum is non-trivial, due to the constraints on the parity of its indices. Ignoring these constraints, as they apparently may have only a sub-leading effect in addressing the asymptotic behaviour of (5.2) in the scaling limit, we thus can write

$$g_{r,s} \sim \kappa_s \sum_{0 < h_1, \dots, h_s < 2r+s-1} \prod_{j=1}^s \alpha^{\frac{1}{2}h_j} \prod_{1 \leq j < k \leq s} |h_k - h_j|.$$

Here, now the h_j s run over all the discrete interval $[1, 2r + s - 2]$ and κ_s is some constant in α , independent of r , but may depend on s .

Summing up, we have rewritten the TDEFP as the partition of a discrete $\beta = 1$ log-gas, consisting in s particles on a lattice, at positions h_j , $j = 1, \dots, s$. The repulsive logarithmic repulsion has a factor $1/2$ with respect to the usual $\beta = 2$ case. The particles are confined to the interval $(0, 2r + s - 1)$ by two ‘hard walls’, and feel a linear potential $-h \log \sqrt{\alpha}$. Recall that $\alpha \in (0, 1)$, implying a positive slope for the potential.

The large s limit of $g_{r,s}$ can be described by the free energy of the log-gas, $\Phi(\theta)$, defined by

$$\Phi(\theta) := - \lim_{s \rightarrow \infty} \frac{1}{s^2} \log g_{\lceil (\theta-1)s/2 \rceil, s}, \quad (5.3)$$

where we have introduced the parameter $\theta := (2r + s)/s$ varying over $(1, \infty)$. The functions $\sigma(\omega)$, defined in (4.3), and $\Phi(\theta)$ are related by

$$\sigma(\omega) = \frac{1}{2} \log \frac{\sqrt{\alpha}}{1 - \alpha} + \Phi(\theta), \quad (5.4)$$

with $\theta = 2/\omega - 1$.

5.2. Limiting cases as $\alpha \rightarrow 0$ and $\alpha \rightarrow 1$. We shall need below, for the full determination of the function $\Phi(\theta)$, the knowledge of its behaviour in the two limiting cases $\alpha \rightarrow 0$ and $\alpha \rightarrow 1$.

In the first case, $\alpha \rightarrow 0$, the weights w_3 and w_4 vanish, and there is only one configuration contributing to both the numerator and the denominator of TDEFP. Therefore, $T_{r,s}|_{\alpha=0} = 1$, implying the behaviour

$$g_{r,s} \sim \alpha^{s(s+1)/4}, \quad \alpha \rightarrow 0,$$

and thus

$$\Phi(\theta) \sim -\frac{1}{4} \log \alpha, \quad \alpha \rightarrow 0. \quad (5.5)$$

The evaluation of the second limit, $\alpha \rightarrow 1$, is slightly more elaborate. This case corresponds to vanishing Boltzmann weights for the vertices of type 1 and 2. It

follows from the definition of TDEFP, requiring to have $s(s+1)/2$ vertices of type 2 in a triangular region in the top-left corner, and from the fact that vertices of type 1 and 2 always come in pairs, that

$$T_{r,s} \sim (1-\alpha)^{s(s+1)/2} C_{r,s}, \quad \alpha \rightarrow 1,$$

where $C_{r,s}$ does not depend on α , and thus

$$\lim_{\alpha \rightarrow 1} g_{r,s} = C_{r,s}.$$

Recalling now the determinant representation (3.5) for $g_{r,s}$, we have:

$$\begin{aligned} C_{r,s} &= \det_{1 \leq j, k \leq s} \left[\operatorname{res}_{x=1} \frac{x^{r+j+k-2}}{(x-1)^{2j}} \right] \\ &= \det_{1 \leq j, k \leq s} \left[\binom{r+j+k-2}{r-j+k-1} \right] \\ &= (-1)^{s(s-1)/2} \det_{1 \leq j, k \leq s} \left[\binom{r+s+k-j-1}{r-s+k+j-2} \right]. \end{aligned}$$

The determinant may be evaluated by resorting to [31], see Theorem 27 therein, yielding:

$$C_{r,s} = \binom{r+s-1}{s} \prod_{j=1}^s \frac{j!}{(2j-1)!} \prod_{1 \leq j < k \leq s} (2r+j+k-2).$$

We are interested into the behaviour of $C_{r,s}$ in the scaling limit, $r, s \rightarrow \infty$, with $2r/s + 1 = \theta$. Let us define

$$\psi(\theta) := - \lim_{s \rightarrow \infty} \frac{1}{s^2} \log C_{\lceil (\theta-1)s/2 \rceil, s}.$$

Using standard arguments based on Stirling formula, we obtain

$$\psi(\theta) := -\frac{1}{4} [(\theta+1)^2 \log(\theta+1) - 2\theta^2 \log \theta + (\theta-1)^2 \log(\theta-1)] + \log 2. \quad (5.6)$$

We thus have

$$\lim_{\alpha \rightarrow 1} \Phi(\theta) = \psi(\theta), \quad (5.7)$$

with $\psi(\theta)$ given by (5.6).

5.3. Solution of the log-gas model. To evaluate the function $\Phi(\theta)$, we follow [21] and introduce the re-scaled variables

$$\mu(x) = \frac{h_j}{s}, \quad x = \frac{j}{s}.$$

These variables satisfy the condition

$$\frac{\mu(y) - \mu(x)}{y - x} \geq 1. \quad (5.8)$$

Sums may now be interpreted as Riemann sums, which, in the large s limit, turns into integrals. We thus have

$$g_{r,s} \propto \int \mathcal{D}[\mu(x)] e^{-s^2 S[\mu(x)]}, \quad r, s \rightarrow \infty,$$

with the action

$$S[\mu(x)] = -\frac{1}{2} \int_0^1 \int_0^1 \log |\mu(y) - \mu(x)| dx dy - \frac{1}{2} \log \alpha \int_0^1 \mu(x) dx.$$

Note that, compared to the situation treated in [10], we have a factor $1/2$ related to the $\beta = 1$ nature of the considered log-gas, and a factor $1/2$ associated to the change of variable (5.1). As a result, the action has an overall $1/2$ factor, and the corresponding saddle-point equation will therefore exactly coincide with the $\beta = 2$ case treated in [10].

We now introduce the density

$$\rho(\mu) = \frac{\partial x(\mu)}{\partial \mu}$$

which must satisfy

$$\int_S \rho(\mu) d\mu = 1, \quad \rho(\mu) \leq 1.$$

where S is the support of the density, $S \subset [0, \theta]$. The first equation is the usual normalization condition, while the second one implements the constraint (5.8).

Next, we introduce the resolvent, which, in the saddle-point approximation, is related to the eigenvalue density as follows

$$W(z) = \int_S \frac{\rho(\mu)}{z - \mu} d\mu, \quad z \notin S.$$

Equivalently, we may express the density as the discontinuity of the resolvent across its cut S ,

$$\rho(z) = -\frac{1}{2\pi i} [W(z + i0) - W(z - i0)], \quad z \in S.$$

Clearly, S is also the support of the density.

In terms of the resolvent, the saddle-point equation reads

$$W(z + i0) + W(z - i0) = 2U(z), \quad z \in S,$$

where, in absence of saturation, $U(z)$ is just the derivative of the potential (i.e., simply $-\log \sqrt{\alpha}$, in our case). The factor 2 in the RHS come from the $\beta = 1$ ensemble of our log-gas. The normalization condition for the density implies for the resolvent the following asymptotic behaviour:

$$W(z) \sim \frac{1}{z} + \frac{E}{z^2} + O(z^{-3}), \quad |z| \rightarrow \infty, \quad (5.9)$$

here E is the the first moment of the density, or, equivalently, the average of the eigenvalues. It is worth emphasizing that, for a linear potential, as it is the case here, the average E and the function $\Phi(\theta)$, see (5.3), are simply related by

$$-2\alpha \partial_\alpha \Phi(\theta) = E. \quad (5.10)$$

Thus the knowledge of the next-to-leading order in the asymptotic expansion of the resolvent at large $|z|$ allows one to determine $\Phi(\theta)$ up to some α -independent quantity.

The presently considered case, with exactly the same saddle-point equation, has been treated in [10]. Due to the linear potential with positive slope, the particles tends to accumulate to the left. As a consequence, we always observe saturation in the vicinity of the origin. Two different scenarios may occur. Given a, b , with $0 < a < b < \theta$, we have:

- *Scenario I* — If the right hard wall is sufficiently far away, there is a saturation for $\mu \in [0, a]$, a band for $\mu \in [a, b]$, and a void for $\mu \in [b, \theta]$;
- *Scenario II* — If the right hard wall is relatively closer, there are two saturated regions for $\mu \in [0, a] \cup [b, \theta]$, and a band for $\mu \in [a, b]$.

For assigned values of α , a phase transition occurs when $\theta = b$. We shall verify below that this condition indeed reproduces the critical value

$$\theta_c = \frac{2}{\omega_c} - 1 = \frac{1 + \sqrt{\alpha}}{1 - \sqrt{\alpha}} \quad (5.11)$$

expected from the correspondence with domino tilings, see (4.4).

Before proceeding we note that our saddle-point equation is exactly the same as in the case of the square EFP [10]. Indeed, the factor 2 in the RHS is compensated by the factor 1/2 in the potential. Conversely, the modifications to the saddle-point equation induced by the possible presence of saturated regions are not affected by this factor 2. But the final form of $\Phi(\theta)$ is, due to the different ‘boundary conditions’ at $\alpha = 0, 1$, with respect to the case of the square EFP.

5.3.1. *Scenario I.* In this case the expression for the resolvent reads

$$W_I(z) = -\log \sqrt{\alpha} - 2 \log \frac{\sqrt{a(z-b)} + \sqrt{b(z-a)}}{\sqrt{(b-a)z}}.$$

The constant a and b are determined by imposing the asymptotic behaviour (5.9) to the resolvent. We have

$$a = \frac{1 - \sqrt{\alpha}}{1 + \sqrt{\alpha}}, \quad b = \frac{1 + \sqrt{\alpha}}{1 - \sqrt{\alpha}}.$$

This scenario requires the presence of a void in the interval $[0, \theta]$. Thus, as θ is decreased, it is clear that the current scenario breaks down at $\theta = \theta_c \equiv b$, as anticipated above.

Evaluation of the next order in the asymptotic behaviour of the resolvent gives

$$E_I = \frac{1 + \alpha}{2(1 - \alpha)},$$

which, after integration, recall (5.10), yields

$$\Phi_I(\theta) = -\frac{1}{2} \log \frac{\sqrt{\alpha}}{1 - \alpha}. \quad (5.12)$$

Note that the condition (5.5) fixes the value of the integration constant to zero.

5.3.2. *Scenario II.* In this case the expression for the resolvent has the following form:

$$W_{II}(z) = -\log \sqrt{\alpha} - \log \frac{z - \theta}{z} - 2 \log \frac{\sqrt{a(z-b)} + \sqrt{b(z-a)}}{\sqrt{\theta - a}\sqrt{z-b} + \sqrt{\theta - b}\sqrt{z-a}}.$$

The requirement of the asymptotic behavior (5.9) for the resolvent leads the following set of equations for the end-points a and b :

$$\begin{aligned} \left(\frac{\sqrt{\theta - a} + \sqrt{\theta - b}}{\sqrt{b} + \sqrt{a}} \right)^2 &= \sqrt{\alpha}, \\ \sqrt{ab} + \sqrt{(\theta - a)(\theta - b)} &= 1. \end{aligned}$$

The solution reads

$$a = \frac{(\sqrt{\theta + 1} - \sqrt{(\theta - 1)\sqrt{\alpha}})^2}{2(1 + \sqrt{\alpha})}, \quad b = \frac{(\sqrt{\theta + 1} + \sqrt{(\theta - 1)\sqrt{\alpha}})^2}{2(1 + \sqrt{\alpha})}. \quad (5.13)$$

The condition $\theta = b$ determines the critical value θ_c , which indeed reproduces (5.11).

Evaluation of the next order in the large $|z|$ behaviour of the resolvent yields:

$$E_{\text{II}} = \frac{a+b}{4} + \frac{\theta}{2} \sqrt{(\theta-a)(\theta-b)}.$$

Substituting here a and b from (5.13), and integrating, see (5.10), we obtain

$$\Phi_{\text{II}}(\theta) = \frac{1}{2}(\theta^2 - 1) \log \frac{2\alpha^{1/4}}{1 + \sqrt{\alpha}} - \frac{1}{4}\theta \log \alpha + \psi(\theta),$$

where $\psi(\theta)$ is given in (5.6). Note that the condition (5.7) fixes the value of the integration constant exactly to $\psi(\theta)$. Expressing α in terms of θ_c , we finally get

$$\begin{aligned} \Phi_{\text{II}}(\theta) = & \frac{1}{2}\theta^2 \log \frac{\theta}{\theta_c} - \frac{1}{4}(\theta-1)^2 \log \frac{\theta-1}{\theta_c-1} - \frac{1}{4}(\theta+1)^2 \log \frac{\theta+1}{\theta_c+1} \\ & + \frac{1}{2} \log \frac{4\theta_c}{\theta_c^2 - 1}. \end{aligned} \quad (5.14)$$

It may be verified that $\Phi(\theta)$ is continuous at $\theta = \theta_c$, together with its first and second derivatives, but has a discontinuity in its third derivative. Such third-order phase transition, in association to the discreteness of a log-gas model, is known as Douglas-Kazakov phase transition [21].

6. Discussion

Recalling that functions $\sigma(\omega)$ and $\phi(\theta)$ are related by (5.4), our expressions (5.12) and (5.14) implies:

$$\sigma(\omega) = 0, \quad \omega \in (0, \omega_c],$$

and

$$\sigma(\omega) = \frac{1}{2} \log \frac{\omega}{\omega_c} - \left(\frac{\omega-1}{\omega} \right)^2 \log \frac{\omega-1}{\omega_c-1} + \frac{1}{2} \left(\frac{\omega-2}{\omega} \right)^2 \log \frac{\omega-2}{\omega_c-2}, \quad \omega \in [\omega_c, 1).$$

The function $\sigma(\omega)$ changes its behaviour at the critical value $\omega_c = 1 - \sqrt{\alpha}$, corresponding to geometric parameters of the pentagonal domain such that the diagonal boundary of the frozen triangle is exactly tangent to the arctic curve of the model.

The leading behaviour of $\sigma(\omega)$ in the vicinity of the point $\omega = \omega_c$,

$$\sigma(\omega) \sim \frac{1}{3(\omega_c-2)(\omega_c-1)\omega_c^3} (\omega - \omega_c)^3, \quad \omega \searrow \omega_c,$$

implies a discontinuity in the third-order derivative. Hence, the function $F(\omega)$, defined in (4.1), has also a discontinuity in its third derivative at $\omega = \omega_c$. In other words, as the scaled size of the cut-off triangle, ω , is varied across the critical value ω_c , a third-order phase transition occurs in the model.

A similar result had already been derived in [10,12], for an L-shaped domain. In that case the cut-off region was a square, or rectangle, and the phase-transition was again triggered by the contact between the cut-off region and the arctic curve. The present result provides further support to the interpretation of the phase separation curves as critical curves in the space of parameters describing the macroscopic geometry of the tiled domain.

The two above mentioned examples of third-order phase transitions observed in domino tilings are clear consequences of the tight connection of these model with discrete log-gases. The mechanism underlying these phase transitions is closely

related to those unveiled in [21, 32, 33] for random matrix models, that have actually reappeared in many different models. See, e.g., [34] for a review.

Concerning the pentagonal domain studied here, note that it slightly differs from that considered in [13]. Indeed, in the present case, the boundary conditions inherited from the six-vertex model introduce some additional comb-like structure along the slanted side, which slightly restrict the possible tilings of the domain, see Fig. 5. Denoting by $\tilde{Z}_{r,s}$ the partition function for the random tilings of the pentagonal domain with no such restriction, one can easily see verify that $\tilde{Z}_{r-1,s+1} < Z_{r,s} < \tilde{Z}_{r,s}$. The microscopic difference between the two domains becomes therefore negligible in the scaling limit considered here.

As a last remark, note that the log-gas representation for EFP, see [10], Eq. (3.4), is in the $\beta = 2$ ensemble, while the representation (3.6) for TDEFP is in the $\beta = 1$ ensemble. This is consistent with the fact that EFP tests the fluctuations of the *intersection* of the arctic curve with the main diagonal, while TDEFP tests the fluctuations of the *maximum* of the arctic curve in the vicinity of the main diagonal. Indeed, these two statistics are known to be governed by the Airy-2 and Airy-1 processes, respectively [13, 35, 36].

Acknowledgments

We are indebted to P. Di Francesco and G. Panova for stimulating discussions. Part of this research was performed while FC was visiting the Institute for Pure and Applied Mathematics (IPAM), which is supported by the National Science Foundation (Grant No. DMS-1925919). AGP acknowledges support from the Theoretical Physics and Mathematics Advancement Foundation BASIS and from the Euler International Mathematical Institute grant No. 075-15-2022-289.

References

- [1] H. Cohn, M. Larsen, and J. Propp, *The shape of a typical boxed plane partition*, New York J. Math. **4** (1998), 137–165, arXiv:math/9801059.
- [2] W. Jockush, J. Propp, and P. Shor, *Random domino tilings and the arctic circle theorem*, arXiv:math/9801068.
- [3] S. Chhita, K. Johansson, and B. Young, *Asymptotic domino statistics in the Aztec diamond*, Ann. Appl. Probab. **25** (2015), 1232–1278, doi:10.1214/14-AAP1021, arXiv:1212.5414.
- [4] R. Kenyon, A. Okounkov, and S. Sheffield, *Dimers and amoebae*, Ann. of Math. **163** (2006), 1019–1056, doi:10.4007/annals.2006.163.1019, arXiv:math-ph/0311005.
- [5] R. Kenyon and A. Okounkov, *Planar dimers and Harnack curves*, Duke Math. J. **131** (2006), 499–524, doi:10.1215/S0012-7094-06-13134-4, arXiv:math/0311062.
- [6] N. Elkies, G. Kuperberg, M. Larsen, and J. Propp, *Alternating-sign matrices and domino tilings (Part 1)*, J. Algebraic Combin. **1** (1992), 111–132, doi:10.1023/A:1022420103267, arXiv:math/9201305.
- [7] N. Elkies, G. Kuperberg, M. Larsen, and J. Propp, *Alternating-sign matrices and domino tilings (Part 2)*, J. Algebraic Combin. **1** (1992), 219–234, doi:10.1023/A:1022483817303, arXiv:math/9201305.
- [8] A. H. Morales, I. Pak, and G. Panova, *Hook formulas for skew shapes IV. Increasing tableaux and factorial Grothendieck polynomials*, J. Math. Sci. **261** (2022), 630–657, doi:10.1007/s10958-022-05777-0, arXiv:2108.10140.
- [9] A. Aggarwal, A. Borodin, and M. Wheeler, *Colored fermionic vertex models and symmetric functions*, Comm. Amer. Math. Soc. **3** (2023), 400–630, doi:10.1090/cams/24, arXiv:2101.01605.
- [10] F. Colomo and A. G. Pronko, *Third-order phase transition in random tilings*, Phys. Rev. E **88** (2013), 042125, doi:10.1103/PhysRevE.88.042125, arXiv:1306.6207.

- [11] V. E. Korepin, *Calculations of norms of Bethe wave functions*, Comm. Math. Phys. **86** (1982), 391–418, doi:10.1007/BF01212176.
- [12] F. Colomo and A. G. Pronko, *Thermodynamics of the six-vertex model in an L-shaped domain*, Commun. Math. Phys. **339** (2015), 699–728, doi:10.1007/s00220-015-2406-9, arXiv: 1501.03135.
- [13] P. L. Ferrari and B. Vetö, *Fluctuations of the arctic curve in the tilings of the Aztec diamond on restricted domains*, Ann. Appl. Probab. **31** (2021), 284–320, doi:10.1214/20-AAP1590, arXiv:1909.10840.
- [14] P. L. Ferrari and B. Vetö, *The hard-edge tacnode process for Brownian motion*, Electron. J. Probab. **22** (2017), 1–32, doi:10.1214/17-EJP97, arXiv:1608.00394.
- [15] S. Delvau and B. Vetö, *The hard edge tacnode process and the hard edge Pearcey process with non-intersecting squared Bessel paths*, Random Matrices Theory Appl. **4** (2015), 1550008, doi:10.1142/S2010326315500082, arXiv:1412.0831.
- [16] F. Colomo and A. G. Pronko, *Emptiness formation probability in the domain-wall six-vertex model*, Nucl. Phys. B **798** (2008), 340–362, doi:10.1016/j.nuclphysb.2007.12.016, arXiv: 0712.1524.
- [17] F. Colomo, A. G. Pronko, and A. Sportiello, *Generalized emptiness formation probability in the six-vertex model*, J. Phys. A: Math. Theor. **49** (2016), 415203, doi:10.1088/1751-8113/49/41/415203, arXiv:1605.01700.
- [18] A. V. Kitaev and A. G. Pronko, *Emptiness formation probability of the six-vertex model and the sixth Painlevé equation*, Commun. Math. Phys. **345** (2016), 305–354, doi:10.1007/s00220-016-2636-5, arXiv:1505.00032.
- [19] I. N. Burenev and A. G. Pronko, *Thermodynamics of the five-vertex model with scalar-product boundary conditions*, Commun. Math. Phys. **405** (2024), 148 (56 pp), doi:10.1007/s00220-024-05021-7, arXiv:2312.17565.
- [20] A. V. Kitaev and A. G. Pronko, *Some explicit results for the generalized emptiness formation probability of the six-vertex model*, J. Math. Sci. **238** (2019), 870–882, doi:10.1007/s10958-019-04282-1.
- [21] M.R. Douglas and V.A. Kazakov, *Large N phase transition in continuum QCD_2* , Phys. Lett. B **319** (1993), 219–230, doi:10.1016/0370-2693(93)90806-S, arXiv:hep-th/9305047.
- [22] A. G. Izergin, *Partition function of the six-vertex model in the finite volume*, Sov. Phys. Dokl. **32** (1987), 878–879.
- [23] A. G. Izergin, D. A. Coker, and V. E. Korepin, *Determinant formula for the six-vertex model*, J. Phys. A **25** (1992), 4315–4334, doi:10.1088/0305-4470/25/16/010.
- [24] V. E. Korepin, N. M. Bogoliubov, and A. G. Izergin, *Quantum inverse scattering method and correlation functions*, Cambridge University Press, Cambridge, 1993.
- [25] F. Colomo and A. G. Pronko, *An approach for calculation of correlation functions in the six-vertex model with domain wall boundary conditions*, Theor. Math. Phys. **171** (2012), 641–654, doi:10.1007/s11232-012-0061-2, arXiv:1111.4353.
- [26] A. G. Pronko, *On the emptiness formation probability in the free-fermion six-vertex model with domain wall boundary conditions*, J. Math. Sci. **192** (2013), 101–116, doi:10.1007/s10958-013-1377-7.
- [27] F. Colomo, G. Di Giulio, and A. G. Pronko, *Six-vertex model on a finite lattice: Integral representations for nonlocal correlation functions*, Nucl. Phys. B **972** (2021), 115535 (42 pp), doi:10.1016/j.nuclphysb.2021.115535, arXiv:2107.13358.
- [28] F. Colomo and A. G. Pronko, *The arctic curve of the domain-wall six-vertex model*, J. Stat. Phys. **138** (2010), 662–700, doi:10.1007/s10955-009-9902-2, arXiv:0907.1264.
- [29] F. Colomo and A. G. Pronko, *Evaluation of integrals for the emptiness formation probability in the square-ice model*, Nucl. Phys. B **1004** (2024), 116565 (28 pp), doi:10.1016/j.nuclphysb.2024.116565, arXiv:2405.04358.
- [30] F. Colomo and A. G. Pronko, *The Arctic Circle revisited*, In: Integrable Systems and Random Matrices: In Honor of Percy Deift, Contemp. Math., vol. 458, Amer. Math. Soc., Providence, RI, 2008, pp. 361–376, doi:10.1090/conm/458/08947, arXiv:0704.0362.
- [31] C. Krattenthaler, *Advanced determinant calculus*, In: The Andrews Festschrift (D. Foata and G.-N. Han, eds.), Springer, Berlin, Heidelberg, 2001, pp. 349–426, doi:10.1007/978-3-642-56513-7_17, arXiv:math/9902004.
- [32] D. J. Gross and E. Witten, *Possible third-order phase transition in the large- N lattice gauge theory*, Phys. Rev. D **21** (1980), 446–453, doi:10.1142/S2010326315500082.

- [33] A. R. Wadia, *$N = \infty$ phase transition in a class of exactly soluble model lattice gauge theories*, Phys. Lett. B **93** (1980), 403–410, doi:10.1016/0370-2693(80)90353-6.
- [34] S. N. Majumdar and G. Schehr, *Top eigenvalue of a random matrix: large deviations and third order phase transition*, J. Stat. Mech. **2014** (2014), P01012, doi:10.1088/1742-5468/2014/01/P01012, arXiv:1311.0580.
- [35] K. Johansson, *The arctic circle boundary and the Airy process*, Ann. Probab. **33** (2005), 1–30, doi:10.1214/00911790400000937, arXiv:math.PR/0306216.
- [36] I. Corwin, J. Quastel, and D. Remenik, *Continuum statistics of the Airy-2 process*, Commun. Math. Phys. **317** (2013), 347–362, doi:10.1007/s00220-012-1582-0, arXiv:1106.2717.

INFN, SEZIONE DI FIRENZE, VIA G. SANSONE 1, I-50019 SESTO FIORENTINO (FI), ITALY
Email address: colomo@fi.infn.it

STEKLOV MATHEMATICAL INSTITUTE, FONTANKA 27, 191023 ST. PETERSBURG, RUSSIA
Email address: a.g.pronko@gmail.com